Linking Morphology and Motion: A Test of a Four-Bar Mechanism in Seahorses*

Gert Roos[1,†]
Heleen Leysen[2]
Sam Van Wassenbergh[1]
Anthony Herrel[1,3]
Patric Jacobs[4]
Manuel Dierick[5]
Peter Aerts[1,6]
Dominique Adriaens[2]
[1]Department of Biology, University of Antwerp, Universiteitsplein 1, B-2610 Antwerp, Belgium; [2]Evolutionary Morphology of Vertebrates, Ghent University, K.L. Ledeganckstraat 35, B-9000 Ghent, Belgium; [3]Department of Organismic and Evolutionary Biology, Harvard University, 26 Oxford Street, Cambridge, Massachusetts 02138; [4]Vakgroep Geologie en Bodemkunde, Ghent University, Krijgslaan 281/S8, B-9000 Ghent, Belgium; [5]Vakgroep Subatomaire en Stralingsfysica, Ghent University, Proeftuinstraat 86, B-9000 Ghent, Belgium; [6]Department of Movement and Sports Sciences, Ghent University, Watersportlaan 2, B-9000 Ghent, Belgium

Accepted 5/2/2008; Electronically Published 11/17/2008

ABSTRACT

Syngnathid fishes (seahorses, pipefish, and sea dragons) possess a highly modified cranium characterized by a long and tubular snout with minute jaws at its end. Previous studies indicated that these species are extremely fast suction feeders with their feeding strike characterized by a rapid elevation of the head accompanied by rotation of the hyoid. A planar four-bar model is proposed to explain the coupled motion of the neurocranium and the hyoid. Because neurocranial elevation as well as hyoid rotation are crucial for the feeding mechanism in previously studied Syngnathidae, a detailed evaluation of this model is needed. In this study, we present kinematic data of the feeding strike in the seahorse *Hippocampus reidi*. We combined these data with a detailed morphological analysis of the important linkages and joints involved in rotation of the neurocranium and the hyoid, and we compared the kinematic measurements with output of a theoretical four-bar model. The kinematic analysis shows that neurocranial rotation never preceded hyoid rotation, thus indicating that hyoid rotation triggers the explosive feeding strike. Our data suggest that while neurocranium and hyoid initially (first 1.5 ms) behave as predicted by the four-bar model, eventually, the hyoid rotation is underestimated by the model. Shortening, or a posterior displacement of the sternohyoid muscle (of which the posterior end is confluent with the hypaxial muscles in *H. reidi*), probably explains the discrepancy between the model and our kinematic measurements. As a result, while four-bar modeling indicates a clear coupling between hyoid rotation and neurocranial elevation, the detailed morphological determination of the linkages and joints of this four-bar model remain crucial in order to fully understand this mechanism in seahorse feeding.

Introduction

Suction feeding is present in most vertebrate groups, including frogs (Dean 2003), salamanders (Elwood and Cundall 1994), turtles (Van Damme and Aerts 1997), and even mammals (Bloodworth and Marshall 2005). However, suction feeding is ubiquitous in some groups, such as teleost fish (Muller and Osse 1984; Lauder 1985) and elasmobranchs (Wilga et al. 2007). The kinematics of suction feeding have been studied and compared between a wide variety of fish (e.g., Carroll and Wainwright 2003; Gibb and Ferry-Graham 2005; Van Wassenbergh et al. 2005). Among the fish species studied, a striking variation in head morphology can be found, ranging from the asymmetrical morphology found in flatfish (Gibb 1997) to the more general laterally compressed percomorph morphology in largemouth bass (Svanbäck et al. 2002) to the extremely elongated upper and lower jaw found in long-jawed butterfly fish (Ferry-Graham et al. 2001). However, despite these great differences in cranial morphology, all these species have converged behaviorally to perform suction feeding.

According to Lauder (1985), prey capture through suction is characterized by four phases: preparation, expansion, compression, and recovery. During the preparation phase, the buccal cavity is compressed and consequently the buccal volume is decreased. In the following expansion phase, the mouth opens quickly through hyoid rotation or through the coupling between the lower jaw, the interhyal, and the operculum. After mouth opening, the suspensorium abducts laterally, and the cranium rotates dorsally. Because of this rapid expansion of the head, the volume in the buccal cavity increases rapidly, sub-

*This paper was a contribution to the symposium "Functional Consequences of Extreme Adaptations of the Trophic Apparatus in Craniates," organized by Dominique Adriaens and Anthony Herrel, at the Eighth International Congress on Vertebrate Morphology, Paris, France, 2007.

†Corresponding author; e-mail: gert.roos@ua.ac.be.

Physiological and Biochemical Zoology 82(1):7–19. 2009. 1522-2152/2009/8201-8043$15.00
DOI: 10.1086/589838

sequently sucking in the prey with the surrounding water. To ensure a continuous posterior flow of water, the expansion movement must proceed from the front to the back of the head. This is often termed the rostrocaudal expansion sequence and is observed in all suction-feeding teleosts studied to date (e.g., Lauder 1985; Carroll and Wainwright 2003; Gibb and Ferry-Graham 2005; Van Wassenbergh et al. 2005). During the compression phase, the mouth of the fish closes, the suspensorium adducts, and the hyoid elevates, together decreasing the volume of the buccal cavity. Finally, the opercular and branchiostegal valves open, allowing the sucked water to flow out of the bucco-pharyngeal cavity through the gill arches. In the last phase, the recovery phase, all the skeletal elements return to their original position.

One of the most extreme cranial morphologies in teleost fish is undoubtedly found in syngnathid fishes (seahorses, pipefish, and sea dragons). These fish are characterized by an elongated tubular snout with minute jaws at its end. Despite this peculiar feeding morphology, it is unclear whether they have converged on the general teleost suction-feeding pattern as mentioned above. However, it is known that seahorses and pipefish use suction to capture their prey (Muller 1987; Bergert and Wainwright 1997; de Lussanet and Muller 2007; Van Wassenbergh et al. 2008). Moreover, their feeding strike is characterized by a very fast rotation of the hyoid and a rapid elevation of the head. Prey capture times within 6 ms are recorded, making them among the fastest suction-feeding vertebrates (Bergert and Wainwright 1997; de Lussanet and Muller 2007; Van Wassenbergh et al. 2008). To execute such extremely rapid movements, Muller (1987) suggested a need for power amplification. More recently, Van Wassenbergh and coworkers (2008) verified that the rapid elevation of the head is probably accomplished by elastic recoil of the tendons of the epaxial muscles.

Muller (1987) also postulated a mechanical linkage between the elevation of the neurocranium and the rotation of the hyoid and described a four-bar linkage model by which the rapid dorsal rotation of the neurocranium could power the expansion of the oropharyngeal cavity and cause explosive suction. The proposed four-bar model consists of the ceratohyal-interhyal complex, the sternohyoideus-urohyal complex, the neurocranium-suspensorium complex, and the pectoral girdle. If this four-bar linkage is kept in a locked position and accompanied by active muscle contraction, elastic energy could potentially be stored and later released. In pipefish, it was originally hypothesized and later demonstrated (Muller 1987; Van Wassenbergh et al. 2008, respectively) that the hyoid is kept in a locked position while the epaxial and hypaxial muscles contract. Through shortening of the muscles, the tendons of the epaxial muscles lengthen and could store elastic energy. A small deviation of the hyoid from its stable position could then trigger the release of previously stored elastic energy, resulting in very fast movements of the head and the hyoid.

In spite of these hypotheses, our understanding of these extremely fast movements is limited because of the relative low temporal resolution of the recordings of the suction event in previous studies (200–400 frames per second [fps], Bergert and Wainwright 1997; 1,000 fps, de Lussanet and Muller 2007; but 2,000 fps, Van Wassenbergh et al. 2008). However, to test the proposed four-bar system, a quantitative analysis of the movements of the cranial elements during the strike is essential. Additionally, a detailed study of the spatial topography and morphology of the joints and linkages of the proposed four-bar system is crucial for our understanding of the functioning of the system.

In this study, we examined the feeding kinematics and cranial morphology in the seahorse species *Hippocampus reidi*, Ginsburg 1933. Quantification of the movements of the cranial elements during prey capture combined with a detailed 3-D analysis of the morphology of the linkages in the proposed four-bar system based on serial histological sections and computed tomography (CT) scanning allows us to test the validity of the model proposed by Muller (1987). Moreover, these data can provide insight on how the extreme suction performance of these animals is achieved.

Material and Methods

Animals

All *Hippocampus reidi* (Ginsburg 1933) were obtained commercially and kept in a large aquarium (300 L) under natural light and photoperiod. Temperature was kept constant at 24°C and salinity at 35 ppt. Because seahorses feed mainly on small crustaceans (Foster and Vincent 2004; Kendrick and Hyndes 2005; Felício et al. 2006), these animals were fed krill, *Artemia*, and *Mysis*, daily. Different animals were used for the morphological analyses and the collection of kinematic data.

Morphology

Specimens used for morphology were killed with an overdose of MS 222 (tricaine methanesulfonate) and fixed in a 4% buffered and neutralized formalin solution. Three specimens of *H. reidi* (11.72 cm, 11.35 cm, and 10.97 cm standard length [SL] and, respectively, 2.38 cm, 2.14 cm, and 2.44 cm head length [HL]) were cleared and stained with alizarin red S and alcian blue according to the protocol of Taylor and Van Dyke (1985). Specimens were dehydrated through a series of alcohol solutions before cartilage staining. Neutralization was done with saturated borax solution followed by bleaching with a 10% solution of H_2O_2 in 0.5% KOH solution and clearing in trypsin enzyme buffer solution (0.45 g in 400 mL of 30% saturated borax solution). Alizarin red S solution was used for bone staining, and specimens were finally preserved in 100% glycerine. On one specimen, dissections were performed on the hyoid for a clearer view of the articulation facets. An Olympus SZX-7 stereoscopic microscope was used for studying the specimens.

Serial Sections

Serial histological cross sections of the head of one specimen (10.35 cm SL, 2.40 cm HL) were made. Before sectioning, the

specimen stored in 70% alcohol was decalcified with 25% Decalc, dehydrated through a graded alcohol series, and embedded in Technovit 7100 (Heraeus Kulzer) according to the Technovit 7100 user instructions. Next, semithin sections (5 μm) were cut using a Leica Polycut SM 2500 sliding microtome equipped with a wolframcarbide-coated knife. Finally they were stained with toluidine blue, mounted with DPX, and covered.

Computed Tomography Scanning

The fifth *H. reidi* specimen (11.90 cm SL, 2.52 cm HL) was scanned at the modular micro-CT setup of Ghent University (Masschaele et al. 2007; http://www.ugct.ugent.be). The source is a dual-head x-ray tube with a transmission type head with a focal spot size of 900 nm below 40 kV tube voltage. The specimen was scanned using the directional tube head, at 80 kV tube voltage. The detector was an a:Si flat panel (Varian Paxscan 2520) with CsI scintillator. In total, 1,000 projections of 748 × 940 pixels were recorded with an exposure time of 1 s per projection and covering 360°. The voxel size in the sample was 61 μm. The raw data were processed and reconstructed using the in-house developed CT software Octopus (Vlassenbroeck et al. 2007) and rendered with VGStudio Max (Volume Graphics, Heidelberg) and Amira 4.1.0 software (Mercury Computer Systems, Mérignac, France).

Graphic 3-D Reconstructions

Computer-generated 3-D reconstructions were made to visualize skeletal (using CT data) and musculoskeletal (using histological sections) topography. Images of the histological sections were captured using a digital camera (Colorview 8, Soft Imaging System) mounted on a Reichert-Jung Polyvar light microscope and controlled by the software program analySIS 5.0 (Soft Imaging System, Münster). The digital images of both CT and histological data were imported in the software package Amira 3.1 (Template Graphics Software, Mérignac, France). Alignment of the histological sections and tracing of the elements was done manually by superimposition to get maximal overlap of all structures. Each element was separately rendered and smoothed and Rhinoceros 3.0 software (McNeel Europe, Barcelona) was used for making composite images of the structures. Only those muscles, tendons, ligaments, and cartilaginous elements related to the hyoid were reconstructed. For the CT data, both volume-rendered and surface-rendered reconstructions were generated of the cranial skeleton.

The 3-D reconstruction, using the histological data, shows a slight distortion at the level of the snout (Fig. 1*C*), which is probably an artifact due to the alignment. Only serial sections of the cranial skeleton were used, so the cleithrum could not be fully reconstructed (Fig. 1*A*, 1*B*).

Kinematics

Two days before a planned filming session, we stopped feeding the animals. During the recording sessions, animals were placed in a smaller tank (305 mm × 200 mm × 50 mm) with a scale bar attached to the tank. At the time of the experiments, five animals were fed small crustaceans (krill, *Artemia*, and *Mysis*) attached to the outflow of a pipette.

Movements of several cranial elements were quantified during prey capture by means of lateral view high-speed video recordings. The video recordings were made using a Redlake Imaging MotionPro digital camera (Redlake, Tucson). Four arrays of eight each red ultrabright LEDs were used for illumination. Sequences were filmed at 2,000 fps with a shutter time of 0.2 ms. Only videos in which the head was oriented perpendicular to the lens of the camera were retained for further analysis (eliminating correction for parallax). A total of 14 recordings from five individuals were used (three videos of four individuals and two of one individual).

Eight landmarks were digitized (Fig. 2) frame by frame using Didge software (A. Cullum, Creighton University, Omaha, NE): (1) the tip of the nose spine, just anterior of the eye; (2) the tip of the snout posterior to the maxillae and premaxillae; (3) the symphysis of the ceratohyals; (4) the tip of the ventrolateral spine on the pectoral girdle; (5) the tip of the process on the second nuchal plate; (6) the upper jaw at the height of the premaxillae; (7) the tip of the lower; and (8) a distinct point on the prey that could be tracked down during the whole sequence (e.g., the eye).

Based on the *X* and *Y* coordinates of these landmarks, five variables were calculated: (*a*) mouth opening (distance 6–7), (*b*) hyoid angle (angle between 1–2 and 3-p, p being the coordinate of the center of the interhyal, of which the position was first determined based on a CT scan and subsequently recalculated for each time step based on the position of the neurocranium landmarks 1–2), (*c*) neurocranial elevation (angle between 1–2 and 4–5), (*d*) cleithrum to hyoid distance (distance 3–4), and (*e*) prey distance (distance 6–8).

In order to reduce digitation noise, the kinematic profiles were filtered using a fourth-order low-pass zero phase shift Butterworth filter with a cutoff frequency of 500 Hz, and velocities and accelerations were calculated through numerical differentiation of the smoothed displacement profiles. The maximal displacements, velocities, and accelerations of each variable were measured as well as the time needed to reach maximal displacements. Time 0 was defined as the image before the first visible movement.

Four-Bar Model

The coupling between the rotation of the neurocranium and the hyoid was evaluated by calculating the output of the planar four-bar system described by Muller (1987). The following landmarks were defined as the joints in the four-bar system (Fig. 2): the center of the interhyal (*p*), the point of articulation of the neurocranium and the vertebral column–pectoral girdle complex (*q*), the medioanterior tip on the cleithrum near the origin of the sternohyoideus muscle (*r*), and the symphysis of the ceratohyals (*s*). CT-scan image reconstructions were used to determine the positions of these four-bar joints relative to

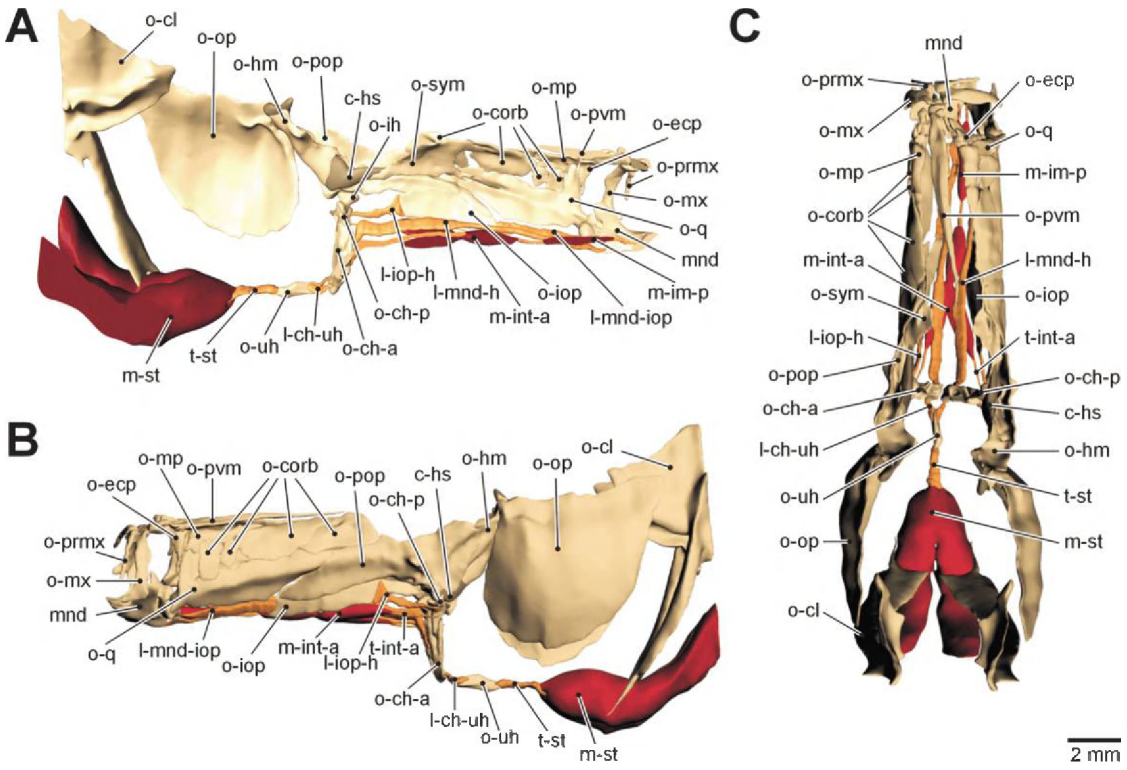

Figure 1. Graphic 3-D reconstruction of the skull of *Hippocampus reidi* (neurocranium not reconstructed). *A*, Medial view of left side. *B*, Lateral view of left side. *C*, Dorsal view. *c-hs*, hyosymplectic cartilage; *l-ch-uh*, ceratohyal-urohyal ligament; *l-iop-h*, interoperculo-hyoid ligament; *l-mnd-h*, mandibulo-hyoid ligament; *l-mnd-iop*, mandibulo-interopercle ligament; *m-im-p*, intermandibularis posterior muscle; *m-int-a*, anterior interhyoideus muscle; *m-st*, sternohyoideus muscle; *mnd*, mandible; *o-ch-a*, anterior ceratohyal; *o-ch-p*, posterior ceratohyal; *o-corb*, circumorbital bones; *o-cl*, cleithrum; *o-ecp*, ectopterygoid; *o-hm*, hyomandibula; *o-ih*, interhyal; *o-iop*, interopercle; *o-mp*, metapterygoid; *o-mx*, maxilla; *o-op*, operacle; *o-pop*, preopercle; *o-prmx*, premaxilla; *o-pvm*, prevomer; *o-q*, quadrate; *o-sym*, symplectic; *o-uh*, urohyal; *t-int-a*, tendon of anterior interhyoideus muscle; *t-st*, tendon of sternohyoideus muscle.

the digitized landmarks on the high-speed video images (Fig. 2). The coordinates of p and q were calculated with respect to a frame of reference defined by two points moving with the neurocranium (landmarks 1–2; Fig. 2). Similarly, the coordinate of r is calculated with respect to landmarks 4–5 (Fig. 2). Finally, because the coordinate of s at time $t = 0$ corresponds to a digitized coordinate (landmark 3; Fig. 2), the initial configuration of the four-bar system at $t = 0$ is set.

From this moment on, the distances of pq, ps, rs, and qr are kept constant. The neurocranium-suspensorium bar qp was chosen as the fixed bar (i.e., the frame). The time-dependent change in the angle between pq and qr equaled the change in the measured neurocranial elevation angle and was used as input motion. The formulas presented in Aerts and Verraes (1984) were used to calculate the resultant rotation of the hyoid with respect to the frame under the four-bar conditions described above. Because the in vivo measured hyoid angle (angle 1–2 to 3-p, Fig. 2) is also available, the four-bar model prediction can be compared with this angle for each time step sampled in the kinematic analysis.

In order to visualize the spatial configuration of the model components before and after neurocranial elevation, the following procedure was executed. Based on the 3-D reconstruction of the CT data, 3-D coordinates (bilateral where possible) were retrieved using Amira 4.1.0 software (Mercury Computer Systems, Mérignac, France) from a selection of 23 articulation points and skeletal reference points (Fig. 3). The coordinates were then imported into Rhinoceros 3.0 software (McNeel Europe SL Barcelona) to construct a simplified model of those structures involved in the hyoid rotation and neurocranial elevation: (1) articulation between lower jaw and quadrate, (2) mandibular symphysis, (3) premaxillary symphysis, (4) rostral tip of prevomer, (5) distal tip of nose spine, (6) articulation between supraoccipital and first nuchal plate (corona), (7) distal tip of the posterior dorsal process on the first nuchal plate, (8) distal tip of the process on the second nuchal plate, (9) articulation between neurocranium and first vertebra, (10) articulation between neurocranium and pectoral girdle, (11) distal tip of the ventrolateral spine on the pectoral girdle, (12) tip of the angle formed between the dorsal horizontal arm of the pectoral girdle and the vertical arm, (13) rostral point of the pectoral complex (formed by the cleithrum and several plates of the bony armor), (14) caudal tip of the urohyal, (15) symphysis of the ceratohyals, (16) articulation between posterior ceratohyal and interhyal, and (17) articulation between interhyal and preopercle.

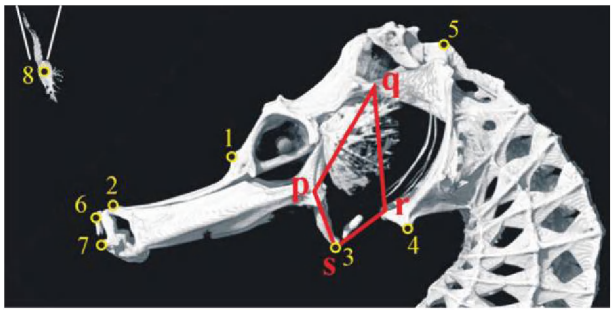

Figure 2. Reconstructed computed tomography data of *Hippocampus reidi* representing the digitized landmarks (*yellow*) and the calculated four-bar system (*red*). The digitized landmarks are (*1*) the distal tip of the nose spine, just anterior to the eye; (*2*) the tip of the snout posterior to the maxillae and premaxillae; (*3*) the symphysis of the ceratohyals; (*4*) the distal tip of the ventrolateral spine on the pectoral girdle; (*5*) the tip of the process on the second nuchal plate; (*6*) the upper jaw; (*7*) the lower jaw; and (*8*) a distinct point on the prey. The point joints of the four-bar system are (*p*) the center of the interhyal, (*q*) the rotation point of the neurocranium with respect to the vertebral column-pectoral girdle complex, (*r*) the medioanterior landmark on the cleithrum, and (*s*) the symphysis of the ceratohyals.

Statistics

In order to statistically determine whether a difference in timing exists between cranial rotation, hyoid rotation, and mouth opening, a contingency table (Fisher's exact test) was used. Data from feeding sequences in which movements occur at the same time frame were omitted from the contingency table. In case a temporal distinction occurs, the contingency table tests whether or not this difference in timing is significant. Note, however, that this statistical test does not rule out that the actual movements might occur at exactly the same instant. This separation of the data set was used only for this specific statistical analysis.

To compare our measurements with the predicted values of the model, a paired *t*-test was used at each time frame to determine at which instant the predicted and the measured values statistically differ. In addition, a least squares regression analysis was used to investigate whether a strong correlation exists in our kinematic data between the angles of hyoid rotation and cranial rotation during the feeding sequence.

Results

Morphology

The terminology of osteological components follows Harrington (1955) and Arratia and Schultze (1990), and the terminology of muscles follows Winterbottom (1974). The following description based on the histological data was confirmed on in toto cleared and stained specimens.

The hyomandibula bears three cartilaginous articulation heads: two dorsally for the sphenotic and prootic and a laterocaudal rounded condyle for the opercle (Fig. 1*A*, 1*C*). Both the opercular and neurocranial processes are surrounded by ligaments. A lateral and a medial wing on the hyomandibula form a groove in which the levator arcus palatine muscle lies dorsally and the preopercle interdigitates with the ventral side of the lateral wing. The hyomandibulo-sphenotic ligament is connected to the distal tip of the lateral wing, and a ligament connected to the parasphenoid attaches on the medial wing. Along its medial length, the hyomandibula is medially provided with a tendinous attachment of the adductor arcus palatine muscle. Rostroventrally, there is a synchondrosis between the hyomandibula and the symplectic (Fig. 1*A*). A firm ligament runs between the hyomandibula and the interhyal. The hyomandibula in *Hippocampus reidi* is not connected to the metapterygoid or interhyal, as it usually is in teleosts (Gregory 1933; Harrington 1955; Rojo 1991). According to Jungersen (1910) the contact between the metapterygoid and the hyomandibula is lost in the families Centriscidae, Aulostomidae, Solenostomidae, and Syngnathidae, whereas Anker (1974) showed that it is still present in *Gasterosteus aculeatus*.

The preopercle is a very long L-shaped dermal bone (Fig. 1*B*). Its horizontal branch stretches out rostrally and is attached to the quadrate and the interopercle through ligaments. Caudally, the vertical branch is tightly connected to the lateral face of the hyomandibula through an interdigitation and connective tissue. Medially, it bears a ridge that supports the symplectic along its length, and the levator arcus palatini muscle fits into a longitudinal groove (Fig. 1*A*). Laterally, it bears a spine. The levator arcus palatini muscle inserts tendinously mediocaudally onto the preopercle. The articulation with the interhyal is situated ventrally where the horizontal and vertical branches meet. Ligaments attached to the ventral surface of the preopercle are those enclosing the joint for the interhyal. The preopercle supports the snout laterally and forms a large part of the suspensorium.

The perichondral interhyal is a small solid bone that bears a lateral and a medial head ventrally (Fig. 4). Dorsocaudally, the rounded cartilaginous surface forms a condyle that fits into the socket joint of the preopercle. In between the lateral and medial process of the interhyal, a saddle joint is formed where the posterior ceratohyal articulates. The lateral process bears ligaments that run to the posterior ceratohyal and preopercle, while massive ligaments from the symplectic and the hyomandibula attach onto the medial head dorsally and ventrally, respectively. Ligaments from both processes thus enclose the joint cavity between the interhyal and the posterior ceratohyal. The plane of the articulatory facet between the preopercle and the interhyal is oriented obliquely. The orientation of the long axis of the interhyal runs from medioventrally to slightly dorsolaterally (Fig. 1*A*).

The perichondral posterior ceratohyal is very irregularly shaped. Apart from the caudal saddle-shaped facet, which articulates in between the two processes of the interhyal, two heads are present on the proximal part of the posterior ceratohyal: a lateral one and a ventral cartilaginous one (Fig. 4). The interoperculo-hyoid ligament, connecting the interopercle with the posterior ceratohyal, attaches rostrally of this lateral process. The slender tendon of the protractor hyoidei muscle runs ventral to the interoperculo-hyoid ligament and attaches

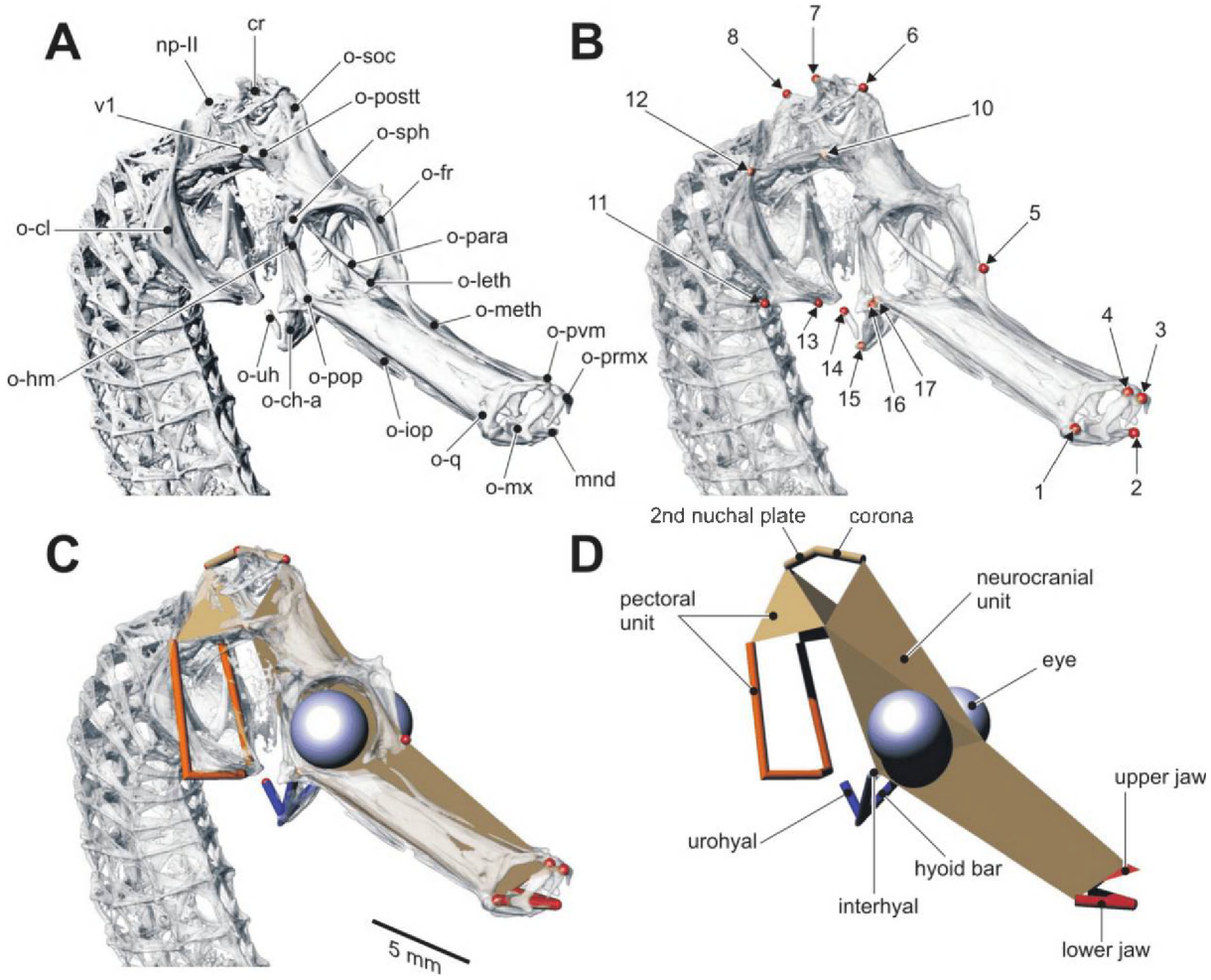

Figure 3. Skull morphology of adult *Hippocampus reidi* and 3-D model. *A*, 3-D reconstruction of the skull based on CT data. *B*, 3-D reconstructions indicating the position of the landmarks used constructing the model (point 9 not illustrated; for a description of the points, see "Material and Methods"). *C*, Model drawn based on the landmarks and superimposed on a 3-D reconstruction. *D*, Model used for visualizing mechanical units and the changes in relative position during feeding strike. *cr*, corona; *np-II*, second nuchal plate; *o-ch-a*, anterior ceratohyal; *o-cl*, cleithrum; *o-fr*, frontal; *o-hm*, hyomandibula; *o-iop*, interopercle; *o-leth*, lateral ethmoid; *o-meth*, mesethmoid; *o-mx*, maxillary; *o-para*, parasphenoid; *o-pop*, preopercle; *o-postt*, posttemporal; *o-prmx*, premaxillary; *o-pvm*, praevomer; *o-q*, quadrate; *o-sph*, sphenotic; *o-soc*, supraoccipital; *o-uh*, urohyal; *mnd*, mandibula; *v1*, first vertebra.

on the lateral side of the posterior ceratohyal (Fig. 1*B*). Its lateral border supports the two slender branchiostegal rays. At its distal end, the posterior ceratohyal bears a thin, tapering process that interdigitates with the anterior ceratohyal. Apart from this interdigitation, there is a firm synchondrotic and ligamentous connection between the anterior and posterior ceratohyals.

The anterior ceratohyal that incorporates the small hypohyal is larger than the posterior one and is more or less triangularly shaped (Fig. 4). The apex of the triangle is situated rostrally, where there is a small but very firm medial symphysis composed of connective tissue between the distal end of the left and right anterior ceratohyal. More proximally, a ligament connects the latter with the very small cartilaginous basihyal. Ventrally, at the apex, a ligament running to the urohyal attaches (Fig. 1). The mandibulo-hyoid ligament runs from the dentary as a single unit along the snout. When it reaches the hyoid, it separates into three parts. All parts attach together medially in a cavity of the anterior ceratohyal. Caudally, the anterior ceratohyal bears several slender processes in between that the long rod of the posterior ceratohyal fits.

The urohyal is a small, more or less cylindrical bone. Rostrally, it bears a thin mediodorsal ridge, giving the urohyal a triangular shape at its front in cross section (Fig. 4). A short and stout ligament attaches on both sides of the ridge and runs to the anterior ceratohyal. The tendon of the sternohyoideus muscle encloses the urohyal caudally (Fig. 1).

The large cleithrum forms the majority of the pectoral girdle. In lateral view, it is roughly comma shaped, with a bigger dorsal part and an anteriorly bent ventral part (Fig. 1*B*). The dorsal component is flattened laterally except for a medial branch that interdigitates firmly with the processus transversus of the first

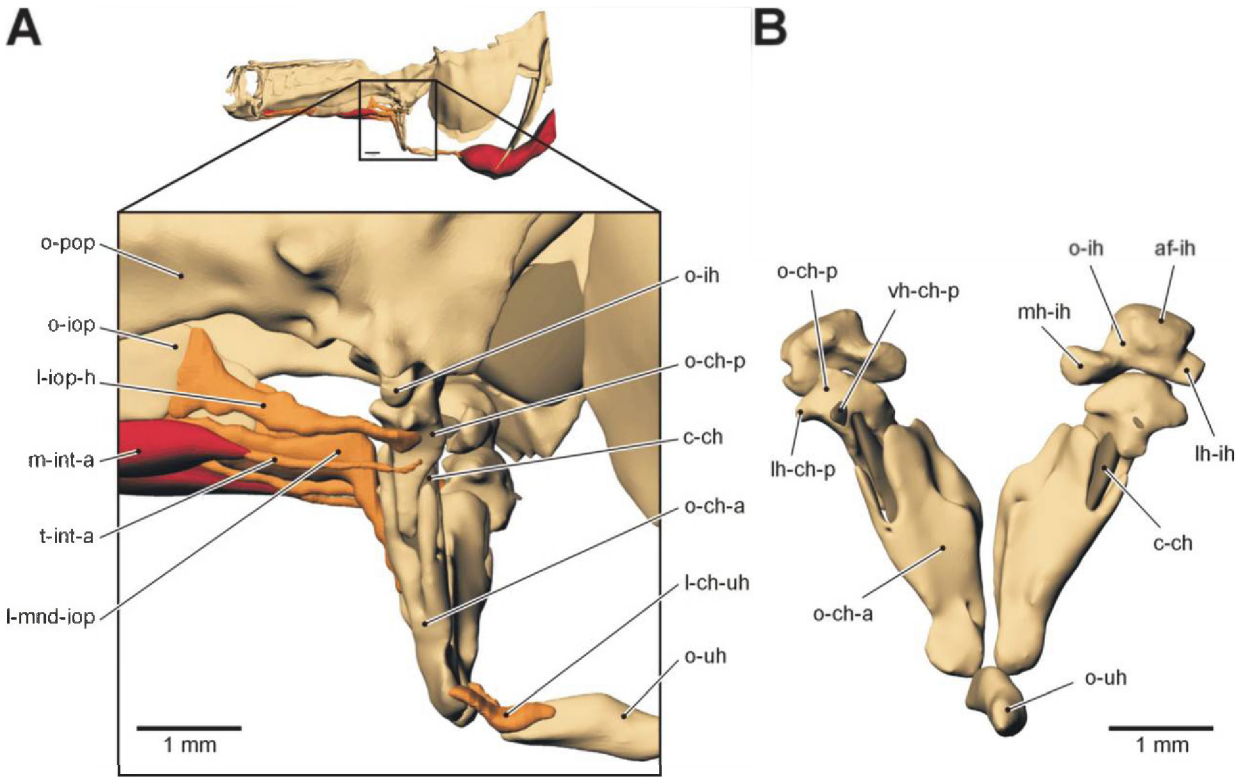

Figure 4. Detail of the 3-D reconstruction of the retracted hyoid complex in *Hippocampus reidi*. *A*, Lateral view of left side. *B*, Caudal view (other structures not reconstructed). *af-ih*, articulation facet of interhyal with preopercle; *c-ch*, ceratohyal cartilage; *l-ch-uh*, ceratohyal-urohyal ligament; *l-iop-h*, interoperculo-hyoid ligament; *l-mnd-iop*, mandibulo-interopercle ligament; *lh-ch-p*, lateral head of posterior ceratohyal; *lh-ih*, lateral head of interhyal; *mh-ih*, medial head of interhyal; *m-int-a*, anterior interhyoideus muscle; *o-ch-a*, anterior ceratohyal; *o-ch-p*, posterior ceratohyal; *o-ih*, interhyal; *o-iop*, interopercle; *o-pop*, preopercle; *o-uh*, urohyal; *t-int-a*, tendon of anterior interhyoideus muscle; *vh-ch-p*, ventral head of posterior ceratohyal.

vertebra (Fig. 1*A*). Laterally, this part is mostly covered by the dorsocaudal edge of the opercle. There is also a dorsocaudal interdigitation with the second nuchal plate, which lies posterior to the corona (first nuchal plate). Anteriorly, a solid ligament runs from the rostral tip of the cleithrum to the caudal end of the exoccipital. This tip fits between the caudal end of the posttemporal laterally and the exoccipital medially, forming the articulation between the pectoral girdle and the neurocranium. A ligamentous connection with the posttemporal, which forms part of the neurocranium in *H. reidi*, is lacking. The ventral part of the cleithrum is bifurcated, with a medial branch contacting the scapulacoracoid and a lateral branch running ventrally, where it interdigitates with the bony armor forming some sort of pectoral complex (Fig. 1*C*). As such, the medial and lateral branches enclose a heart-shaped cavity into which lies the sternohyoid muscle and pectoral fin musculature. These two branches fuse more caudally and form a bony sheet dorsal to the muscles.

The protractor hyoidei muscle is generally considered to be embryologically formed by the fusion of the intermandibularis posterior and the anterior interhyoideus muscle (Winterbottom 1974), but see Geerinckx and Adriaens (2007) for a discussion of possible misinterpretations on the true nature of this muscle. In *H. reidi*, however, both parts can still be clearly distinguished from each other because they are well separated by a tendinous connection (Fig. 1*C*). Rostrally, two short tendons are connected to the medial face of the left and right dentary, ventral to the anterior intermandibularis muscle (connecting the two dentaries). The posterior intermandibularis part starts as two individual bundles of fibers fusing almost halfway along their length when reaching the tendinous connection. Fibers of both the posterior intermandibularis and the anterior interhyoideus muscle run in a longitudinal direction. Although not visible on the reconstruction, the serial sections show that along its entire length, the anterior interhyoideus consists of two bundles separated in the middle by a thin layer of connective tissue. More caudally, the bundles diverge, giving the muscle its typical X shape. Attachment by a long and slender tendon occurs on the lateral face of the posterior ceratohyal, just ventral to attachment of the interoperculo-hyoid ligament (Figs. 1*B*, 4*A*).

The sternohyoideus muscle inserts anteriorly on the urohyal by a firm tendon that caudally splits into two and continues to run in between the fibers (Fig. 1). The muscle is enclosed by ventral bony plates of the body and partly by the lateral and medial branch of the cleithrum nearly along its entire length. More caudally, the bony armor extends laterally, with the pectoral fin musculature being situated dorsally. The site of origin of the sternohyoideus is the cleithrum, the scapulacoracoid,

Table 1: Summary kinematics of the prey capture event in *Hippocampus reidi* ($N = 14$)

Variable	Mean	SE
Peak hyoid rotation (°)[a]	68.45	4.32
Peak velocity hyoid rotation (°/s)	29.85×10^3	2.42×10^3
Peak acceleration hyoid rotation (°/s^2)	23.22×10^6	1.84×10^6
Onset hyoid rotation (ms)	.50	.00
Time to peak hyoid rotation (ms)	17.29	1.58
Time to peak velocity hyoid rotation (ms)	1.29	.07
Time to peak acceleration hyoid rotation (ms)	.50	.00
Peak cranial elevation (°)[a]	31.10	2.13
Peak velocity cranial elevation (°/s)	13.88×10^3	976.77
Peak acceleration cranial elevation (°/s^2)	10.36×10^6	709.71×10^3
Onset cranial elevation (ms)	.64	.08
Time to peak cranial elevation (ms)	18.46	1.59
Time to peak velocity cranial elevation (ms)	1.36	.06
Time to peak acceleration cranial elevation (ms)	.50	.00
Peak mouth opening (mm)[a]	2.70	.16
Peak velocity mouth opening (m/s)	1.58	.12
Peak acceleration mouth opening (m/s^2)	1.22×10^3	116.53
Onset of mouth opening (ms)	.75	.07
Time to peak mouth opening (ms)	3.50	.28
Time to peak velocity mouth opening (ms)	1.21	.09
Time to peak acceleration mouth opening (ms)	.46	.04
Peak shortening pectoral girdle–certatohyal tip (mm)[a]	1.05	.18
Peak velocity shortening pectoral girdle–certatohyal tip (m/s)	55.12	8.45
Peak acceleration shortening pectoral girdle–certatohyal tip (m/s^2)	70.24×10^3	7.80×10^3
Onset of shortening pectoral girdle–ceratohyal (ms)	.82	.19
Time to peak shortening pectoral girdle–certatohyal tip (ms)	12.80	.25
Time to peak velocity shortening pectoral girdle–certatohyal tip (ms)	.54	.18
Time to peak acceleration shortening pectoral girdle–certatohyal tip (ms)	.20	.05
Duration of prey capture (ms)	5.50	.44
Prey distance at time 0 (mm)	6.71	.53
Peak velocity prey (m/s)	.27	.06
Peak acceleration prey (m/s^2)	190.37	57.62
Time to peak velocity prey (ms)	5.10	.86
Time to peak acceleration prey (m/s^2)	4.00	.91

[a] Calculated as the difference between the value at time 0 ms and the maximum value.

and the ventral bony plates onto which the sternohyoideus attaches through a layer of connective tissue. The two large and firm bundles of the sternohyoideus muscle course rostroventrally and unite anteriorly. Caudally they join the fibers of the hypaxial muscle.

Kinematics

During the preparatory phase, the animal approaches its prey relatively slowly. Next, the expansion phase, is characterized by a fast rotation of the hyoid and a rotation of the head and snout. The mouth starts to open a few milliseconds later (Table 1; Fig. 5). Cranial elevation causes the mouth opening to be positioned in close proximity to and directed toward the prey, which is finally sucked into the mouth. After prey capture, a relatively long period is needed to restore the original configuration of the skeletal elements (Fig. 5).

The cranium starts to elevate 0.14 ± 0.08 ms (mean $\pm$ SE) after the onset of hyoid rotation (Table 1; Fig. 6). In eight of the 14 analyzed sequences, feeding began with hyoid rotation. In six sequences, hyoid rotation and neurocranial elevation started at the same video image. Therefore, the onset of neurocranial elevation did not preceded the onset of hyoid rotation in any of the sequences. Consequently, in the eight sequences where a clear temporal distinction between both movements is present, the onset of hyoid rotation is significantly earlier than the onset of neurocranial elevation (Fisher's exact test, $P = 0.04$) This result was supported by preliminary data based on videos recorded at 8,000 fps.

The onset of mouth opening takes place 0.11 ± 0.01 ms after the onset of neurocranial elevation (and thus 0.25 ± 0.07 ms after the onset of hyoid rotation). The onset of cranial elevation preceded the onset of mouth opening in 10 of the 14 sequences.

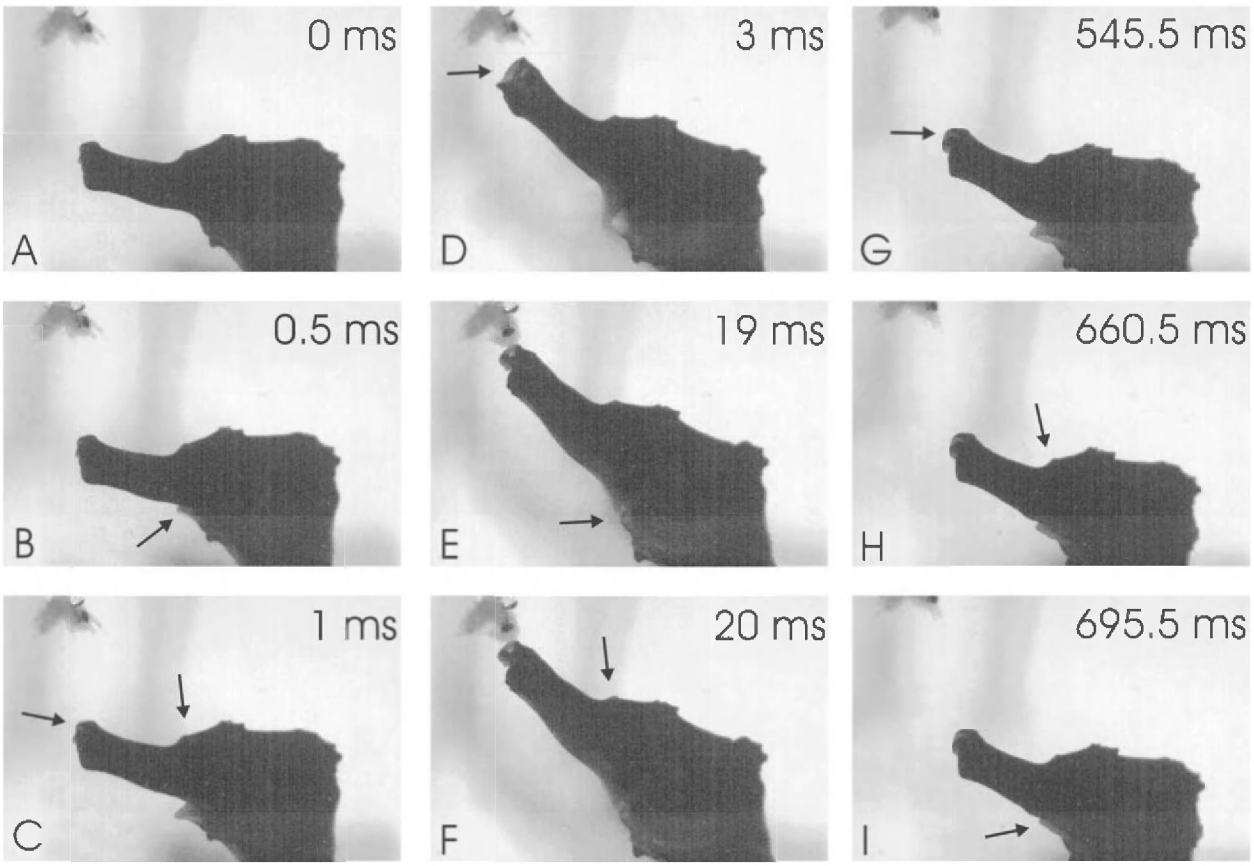

Figure 5. Example of a feeding sequence of *Hippocampus reidi* feeding on a mysid shrimp in the upper-left corner. Important events are indicated by an arrow. *A*, Image of one frame just before the first visible movement. *B*, Onset of hyoid rotation. *C*, Onset of cranial rotation and mouth opening. *D*, Mouth reaches maximal opening. *E*, Hyoid reaches maximal rotation. *F*, Neurocranium reaches maximal rotation. *G*, Mouth fully closed. *H*, Neurocranium restored to its original position. *I*, Hyoid fully protracted.

In the four remaining sequences, the onsets of neurocranial elevation and mouth opening occurred at the same video image. Consequently, the onset of neurocranial elevation is significantly earlier on average than the onset of mouth opening (Fisher's exact test, $P = 0.02$) in 10 videos where a clear temporal distinction was apparent. Mouth opening reaches a peak value of 0.27 ± 0.16 cm 3.50 ± 0.28 ms after the beginning of hyoid rotation.

The prey is sucked in 2.00 ± 0.16 ms after the mouth reaches its maximum gape (5.50 ± 0.44 ms after the onset of hyoid rotation). Next, the hyoid reaches its peak excursion of 68.45° ± 4.32° 17.29 ± 1.58 ms after the onset of hyoid rotation. The neurocranium is the last element reaching its peak elevation of 31.10° ± 2.13° 18.46 ± 1.59 ms after the onset of hyoid rotation. During the entire feeding strike, there exists a strong correlation between the cranial elevation and the hyoid rotation (correlation test, $N = 51$, $R^2 = 0.99$, $P < 0.01$).

The duration of the expansion phase (which begins with the onset of hyoid rotation and ends with the beginning of mouth closing) is 5.77 ± 0.66 ms. The compression phase (which is defined here as starting at the onset of mouth closing and ending when the mouth is fully closed) lasts much longer, with a duration of 415.74 ± 48.20 ms. The final recovery phase (which begins at the moment the jaws are fully closed and ends at the time all skeletal elements have acquired their original position) has a duration of 168.23 ± 36.27 ms. The total duration of the feeding sequence (beginning one frame before the onset of hyoid rotation and ending at the end of the recovery phase) is 598.73 ± 25.12 ms, on average.

Four-Bar Model

The hyoid angle calculated through the four-bar model reaches a maximum peak of 88.99° ± 5.29° (mean ± SE) after 18.46 ± 1.49 ms. The measured hyoid angle is on average 10.99° larger, while the timing of peak excursion differs only by 1.17 ms (Fig. 7). During the first 1.50 ms, the measured hyoid angle statistically shows no difference from the predicted hyoid angle (*t*-test, $t = 1.514$, df = 13, $P = 0.154$). After this initial phase, the predicted angle started to underestimate the measured hyoid angle significantly (*t*-test, $t = 3.034$, df = 13, $P < 0.01$ after time = 2.00 ms) and finally ends at 91.08% of the measured angle (Fig. 7). This pattern is consistently observed for each individual feeding sequence analyzed.

The morphological analysis confirms that the neurocranium and the suspensorium can be represented as a single unit (as

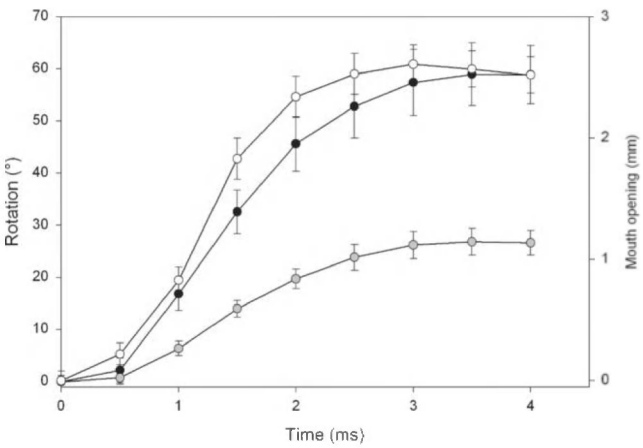

Figure 6. Time-averaged kinematic profiles ($N = 14$) of the mean hyoid rotation (*black dots*), the mean neurocranial rotation (*gray dots*), and the mean mouth opening (*white dots*) of all 14 sequences. Time = 0 ms was consequently defined for each sequence as the frame before the first visible movement. Prey capture occurs on average 5.5 ms after the onset of hyoid rotation.

assumed in the four-bar model) articulating with the following structures: the pectoral girdle, the vertebral column, the ceratohyals (through the interhyals), and the lower jaws (Fig. 8). The upper jaws articulate with the neurocranium, but with respect to the four-bar linkage system, they can be considered as mechanically coupled to the neurocranial unit. The degrees of freedom between the neurocranium, pectoral girdle, and vertebral column are reduced because the vertebral column is immovably connected to the pectoral girdle. As such, the pectoral girdle can be considered to be part of the postcranial skeletal unit. This also implies that this postcranial skeletal unit articulates with the neurocranium with three joints: two for the pectoral girdle and one for the first vertebra. All three joints show a topography where they are well aligned (so the vertebral articulation is lining up with the axis between the left and right pectoral articulation).

As neurocranial rotation must occur around the axis going through the three neurocranial joints, its elevation is coupled to a posterior displacement of the supraoccipital crest with respect to the nuchal plates. As the second nuchal plate is strongly connected to both the pectoral girdle and the neural spine of the first vertebra, a posterior rotation of the supraoccipital crest must be compensated for by a sliding or tilting action of the corona, the first nuchal plate, with respect to the second one and/or the neurocranium. At this point, it cannot be discerned whether this movement involves one or both actions, but the model does suggest that a forward movement of the corona with respect to the supraoccipital crest occurs (indicated by the shortened distance of the bar connecting the supraoccipital crest and the distal tip of the process on the corona; Fig. 8*B*).

Using the image of a feeding *H. reidi* at the maximum of neurocranial elevation, where the depressed hyoid bars could clearly be observed, the model could only be fitted properly if the interhyals were rotated forward (thus contrary to what would be expected for hyoid rotation). Observations of dissected specimens also indicated the interhyal to be directed rostrally when the hyoid is depressed. Whether or not the interhyal is also directed rostrally at the onset of neurocranial elevation could not be determined based on the model (Fig. 8).

Discussion

Comparison with Other Teleosts

A comparison of the kinematics of the feeding strike of *Hippocampus reidi* with the rostrocaudal expansion sequence of typical suction-feeding teleosts reveals differences in the timing of the movements of the skeletal components. When there was a clear temporal distinction, the hyoid (and not the mouth, as observed for typical teleost suction feeders; see, e.g., Lauder 1985; Carroll and Wainwright 2003; Gibb and Ferry-Graham 2005; Van Wassenbergh et al. 2005) in *H. reidi* is the first component of the cranial system that is set in motion. However, in six of a total 14 sequences, hyoid rotation and cranial elevation occur at the same time frame; therefore, we cannot statistically justify whether or not a difference in timing exist. In those cases where our temporal resolution was adequate and the two behaviors showed temporal separation, hyoid movements always preceded cranial rotation. Considering the very fast movements, this apparent overlap in timing could be caused by the low temporal resolution of the recordings. Therefore, further analyses using higher temporal resolution are needed to confirm this finding and test its generality. The mouth is directed to the prey via cranial elevation, which occurs just after the onset of hyoid rotation. Cranial elevation thus appears to be used for positioning the mouth opening toward the prey rather than contributing to mouth opening (also found

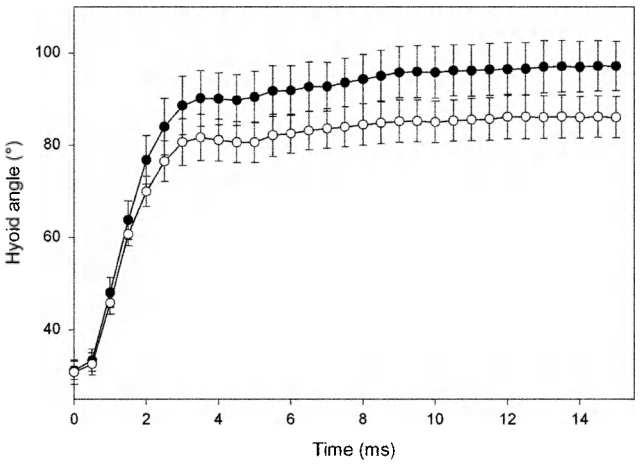

Figure 7. Comparison of the average measured hyoid angle (*black dots*) and the average hyoid angle predicted by the four-bar model (*white dots*; $N = 14$). In the first 1.5 ms, the graphs do not statistically differ (t-test, $t = 1.514$, df = 13, $P > 0.05$); at time = 2 ms, the graphs significantly diverge (t-test, $t = 3.034$, df = 13, $P < 0.05$).

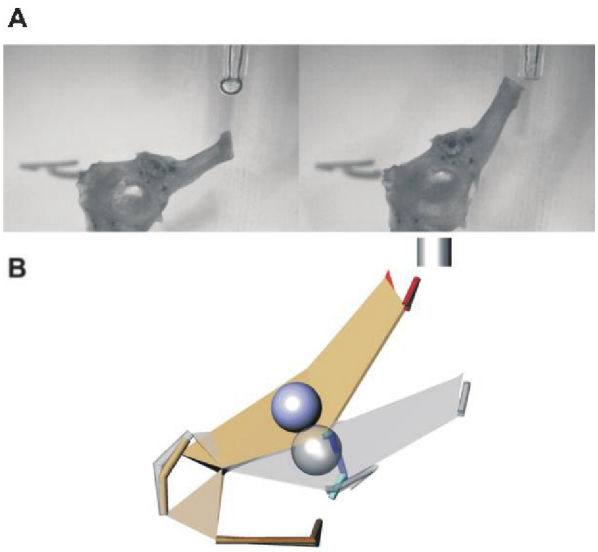

Figure 8. Model showing extensive neurocranial elevation in *Hippocampus reidi*. *A*, Video frames used for positioning the components of the model at the onset of neurocranial elevation (*left*) and at maximal elevation (*right*). *B*, Model at onset of elevation. *C*, Position of skull at maximal elevation superimposed and aligned based on the position of the pectoral girdle.

in clariid catfish; Van Wassenbergh et al. 2006), which also differs from the typical teleost pattern (e.g., Lauder 1985). Prey capture occurred within 5–6 ms, which makes *H. reidi* one of the fastest suction feeders to date, comparable with the reported prey capture times of antennariid anglerfish (Grobecker and Pietsch 1979).

Kinematics and Morphology Related to the Four-Bar Mechanism

The four-bar linkage proposed by Muller (1987) consists of the neurocranium-suspensorium complex, the hyoid, the sternohyoideus-urohyal complex, and the vertebral column–pectoral girdle complex. In *H. reidi*, the articulation between the suspensorium and the hyoid is provided by the interhyal. In a generalized teleost, this small bone is usually rod shaped and bears a rounded head that fits into a facet of the suspensorium, forming a ball-and-socket joint (Anker 1989; Aerts 1991). This configuration permits the interhyal to rotate in every direction with respect to the suspensorium (unless restricted by the suspensorium itself). In *H. reidi*, however, the interhyal is reduced to only the ball of the ball-and-socket joint, which bears two distinct ventral processes (Fig. 4). The posterior ceratohyal, forming a rigid unit with the anterior ceratohyal, articulates in between these heads. The two heads of the interhyal reduces the degrees of freedom between the hyoid and the suspensorium. Thus, movements are largely confined to a sagittal plane going through the long axis of the interhyal. This movement is very important for hyoid rotation during the expansion phase of suction feeding (Aerts 1991). The morphological specialization of the interhyal does suggest that this bone and its movements play an important role in the suction-feeding mechanism and cannot be neglected.

The hyoid bar and the sternohyoideus-urohyal complex are connected through a ligament that runs from the ventral apex of the anterior ceratohyal to the mediodorsal ridge of the urohyal (Figs. 1, 4). The attachment of this ligament is the position where the force is applied during sternohyoid contraction. As the distance between the attachment and the rotation center (the articulation with the interhyal) is maximal, the moment arm and, as a consequence, the moment of force will be large as the hyoid becomes depressed (and thus the angle between the hyoid and the sternohyoideus becomes more favorable). Caudally, the tendon of the sternohyoideus muscle encloses the urohyal. Surprisingly, several figures in Muller (1987) show a working line of the sternohyoid muscle forming an angle with the urohyal. This is in contradiction to his previous definition of the sternohyoideus-urohyal complex, which comprises the sternohyoideus muscle and the urohyal as a single bar. Also, anatomically, this is impossible, because the urohyal in teleosts typically ossifies within the tendon of the sternohyoideus and will therefore always be positioned in the working line of this muscle (and thus in the line through the tendon; De Beer 1937; Patterson 1977).

Our comparison between the results of the four-bar system (Muller 1987) and the observed kinematics showed good agreement during the first 1.5 ms of the feeding strike (Fig. 7). After the initial 1.5 ms, the trajectories started to diverge, and a clear difference between the two movement profiles becomes apparent. Given the above morphological considerations, this is most likely caused by shortening of the sternohyoideus-urohyal "bar" (*rs* in Fig. 2). Indeed, calculating the distance between the hyoid and the tip of the cleithrum shows an average shortening of 1.54 mm. A second possible explanation of the discrepancy between the four-bar model and the measured kinematics (Fig. 7) is abduction of the hyomandibula; because this implies a lateral (outward) displacement of the interhyal joint, the projected length of the ceratohyals on the dorsoventral plane (i.e., the four-bar plane) will decrease. However, calculating the distance between the hyoid tip and the interhyal in the dorsoventral plane never showed a significant decrease during the phase of rapid neurocranial elevation. Therefore, it appears that defining the sternohyoideus-urohyal complex as a bar of constant length and not suspensorium abduction is responsible for the underestimation of the actual rotation of the hyoid. It should also be noted that given the functional continuum of the sternohyoideus and the hypaxial muscles in *H. reidi*, hypaxial muscle shortening may contribute to the observed decrease in length between the hyoid tip and the cleithrum tip.

Due to the immobile connection between the pectoral girdle and the vertebrae, the pectoral girdle and vertebral column should be considered a single mechanical unit (at least with respect to the four-bar linkage system). This simplification has also been made by Muller (1987); he eliminates the movable connection between the pectoral girdle and neurocranium and continues to work with the vertebra-neurocranium articulation.

This configuration seems to indicate a strengthened but mobile connection between neurocranium and vertebral system by this pectoral-vertebral ankylosis, as the neurocranio-vertebral articulation lies onto the axis connecting the left and right pectoral articulations with the neurocranium. From a mechanical point of view, any deviation from this axis would be prone to a dislocation during extensive neurocranial elevation.

According to Bergert and Wainwright (1997), the components of the Muller four-bar linkage model are the hyomandibula, the ceratohyal, the sternohyoideus muscle together with the urohyal, and the pectoral girdle. They give a description of the *Hippocampus erectus* skull, with the hyomandibula covering the preopercle and articulating with the interhyal (Bergert and Wainwright 1997). However, this configuration cannot be found in *H. reidi*, *Hippocampus capensis*, or *Hippocampus kuda*.

Final Conclusion

In conclusion, our morphological and kinematic data clearly show an important coupling between the hyoid rotation and neurocranial elevation in *H. reidi*, as suggested by Muller's four-bar mechanism (1987). However, our results do show a significant difference between the model and the observed kinematics near the end of the neurocranial elevation phase, which points out that the model does not entirely describe the actual movements during a feeding strike in *H. reidi*. Because the sternohyoideus runs through the pectoral girdle and is confluent with the hypaxial musculature, modeling the sternohyoideus-urohyal complex as a bar of constant length is not appropriate. Our data show that the extreme performance of the feeding system in seahorses is made possible through a series of morphological specializations of the cranial system.

Acknowledgments

Research for this article was supported by Fonds voor Wetenschappelijk Onderzoek (Funds for Scientific Research; FWO) grant G 053907. G.R. and H.L. are funded by a PhD grant of the Instituut voor de Aanmoediging van Innovatie door Wetenschap en Technologie in Vlaanderen (Institute for the Promotion of Innovation by Science and Technology in Flanders). S.V.W. is postdoctoral fellow of the FWO, Flanders. Special thanks to Barbara De Kegel and Joachim Christiaens for making the serial histological sections.

Literature Cited

Aerts P. 1991. Hyoid morphology and movements relative to abducting forces during feeding *Astatotilapia elegans* (Teleostei: Cichlidae). J Morphol 208:323–346.

Aerts P. and W. Verraes. 1984. Theoretical analysis of a planar four-bar linkage in the teleostean skull: the use of mathematics in biomechanics. Ann Soc R Zool Belg 114:73–290.

Anker G.C. 1974. Morphology and kinetics of the head of the stickleback, *Gasterosteus aculeatus*. Trans Zool Soc Lond 32: 311–416.

———. 1989. The morphology of joints and ligaments of a generalized *Haplochromis*species: *H. elegans* Trewavas 1933 (Teleostei, Cichlidae). III. The hyoid and the branchiostegal apparatus, the branchial apparatus and the shoulder girdle apparatus. Neth J Zool 39:1–40.

Arratia G. and H.-P. Schultze. 1990. The urohyal: development and homology within osteichthyans. J Morphol 203:247–282.

Bergert B.A. and P.C. Wainwright. 1997. Morphology and kinematics of prey capture in the syngnathid fishes *Hippocampus erectus* and *Syngnathus floridae*. Mar Biol 127:563–570.

Bloodworth B. and C.D. Marshall. 2005. Feeding kinematics of *Kogia* and *Tursiops* (Odontoceti: Cetacea): characterization of suction and ram feeding. J Exp Biol 208:3721–3730.

Carroll A.M. and P.C. Wainwright. 2003. Functional morphology of prey capture in sturgeon, *Scaphirhynchus albus*. J Morphol 256:270–284.

Dean M.N. 2003. Suction feeding in the pipid frog, *Hymenochirus boettgeri*: kinematic and behavioral considerations. Copeia 4:879–886.

De Beer G.R. 1937. The Development of the Vertebrate Skull. Clarendon, Oxford.

de Lussanet M.H.E. and M. Muller. 2007. The smaller your mouth, the longer your snout: predicting the snout length of *Syngnathus acus*, *Centriscus scutatus* and other pipette feeders. J R Soc Interface 4:561–573.

Elwood J.R.L. and D. Cundall. 1994. Morphology and behavior of the feeding apparatus in *Cryptobranchus alleganiensis* (Caudata). J Morphol 220:47–70.

Felício A.K.C., I.L. Rosa, A. Souto, and R.H.A. Freitas. 2006. Feeding behavior of the longsnout seahorse *Hippocampus reidi* Ginsburg, 1933. J Ethol 24:219–225.

Ferry-Graham L.A., P.C. Wainwright, and D.R. Bellwood. 2001. Prey capture in long-jawed butterflyfishes (Chaetodontidae): the functional basis of novel feeding habits. J Exp Mar Biol Ecol 256:167–184.

Foster S.J. and A.C.J. Vincent. 2004. Life history and ecology of seahorses: implications for conservation and management. J Fish Biol 65:1–61.

Geerinckx T. and D. Adriaens. 2007. Ontogeny of the intermandibular and hyoid musculature in the suckermouth armoured catfish *Ancistrus* cf. *triradiatus* (Loricariidae, Siluriformes). Anim Biol 57:339–357.

Gibb A.C. 1997. Do flatfish feed like other fishes? a comparative study of percomorph prey-capture kinematics. J Exp Biol 200:2841–2859.

Gibb A.C. and L.A. Ferry-Graham. 2005. Cranial movements during suction feeding in teleost fishes: are they modified to enhance suction production? Zoology 108:141–153.

Gregory W.K. 1933. Fish skulls: a study of the evolution of natural mechanics. Trans Am Philos Soc 23:75–481.

Grobecker D.B. and T.W. Pietsch. 1979. High-speed cinematographic evidence for ultrafast feeding in antennariid anglerfishes. Science 205:1161–1162.

Harrington R.W. 1955. The osteocranium of the American cyp-

rinid fish, *Notropis bifrenatus*, with an annoted synonymy of teleost skull bones. Copeia 4:267–290.

Jungersen H.F.E. 1910. Ichthyological Contributions. II. The Structure of the Aulostomidae, Syngnathidae and Solenostomidae. Det Kongelige Danske Videnskabernes Selskabs skrifter, Raekke 7. Köbenhaven.

Kendrick A.J. and G.A. Hyndes. 2005. Variations in the dietary compositions of morphologically diverse syngnathid fishes. Environ Biol Fish 72:415–427.

Lauder G.V. 1985. Aquatic feeding in lower vertebrates. Pp. 210–229 in M. Hildebrand, D.M. Bramble, K.F. Liem, and D.B. Wake, eds. Functional Vertebrate Morphology. Harvard University Press, Cambridge, MA.

Masschaele B.C., V. Cnudde, M. Dierick, P. Jacobs, L. Van Hoorebeke, and J. Vlassenbroeck. 2007. UGCT: new x-ray radiography and tomography facility. Nucl Instrum Methods Phys Res A 580:266–269.

Muller M. 1987. Optimization principles applied to the mechanism of neurocranium elevation and mouth bottom depression in bony fishes (Halecostomi). J Theor Biol 126:343–368.

Muller M. and J.W.M. Osse. 1984. Hydrodynamics of suction feeding in fish. Trans Zool Soc Lond 37:51–135.

Patterson C. 1977. Cartilage bones, dermal bones and membrane bones, or the exoskeleton *versus* the endoskeleton. Pp. 77–121 in S.M. Andrews, R.S. Miles, and A.D. Walker, eds. Problems in Vertebrate Evolution. Academic Press, London.

Rojo A.L. 1991. Dictionary of Evolutionary Fish Osteology. CRC, Boca Raton, FL.

Svanbäck R., P.C. Wainwright, and L.A. Ferry-Graham. 2002. Linking cranial kinematics, buccal pressure, and suction feeding performance in largemouth bass. Physiol Biochem Zool 75:532–543.

Taylor W.R. and G.C. Van Dyke. 1985. Revised procedures for staining and clearing small fishes and other vertebrates for bone and cartilage study. Cybium 9:107–119.

Van Damme J. and P. Aerts. 1997. Kinematics and functional morphology of aquatic feeding in Australian snake-necked turtles (Pleurodira; Chelodina). J Morphol 233:113–125.

Van Wassenbergh S., A. Herrel, D. Adriaens, and P. Aerts. 2005. A test of mouth-opening and hyoid-depression mechanisms during prey capture in a catfish using high-speed cineradiography. J Exp Biol 208:4627–4639.

———. 2006. Modulation and variability of prey capture kinematics in clariid catfishes. J Exp Zool 305A:559–569.

Van Wassenbergh S., J.A. Strother, B.E. Flammang, L.A. Ferry-Graham, and P. Aerts. 2008. Extremely fast prey capture is powered by elastic recoil. J R Soc Interface 5:285–296.

Vlassenbroeck J., M. Dierick, B. Masschaele, V. Cnudde, L. Van Hoorebeke, and P. Jacobs. 2007. Software tools for quantification of x-ray microtomography at the UGCT. Nucl Instrum Methods Phys Res A 580:442–445.

Wilga C.D., P.J. Motta, and C.P. Sanford. 2007. Evolution and ecology of feeding in elasmobranchs. Integr Comp Biol 47: 55–69.

Winterbottom R. 1974. A descriptive synonymy of the striated muscles of the Teleostei. Proc Acad Nat Sci Phila 125:225–317.